RSC Advances

PAPER

View Article Online
View Journal | View Issue

Cite this: *RSC Adv.*, 2026, **16**, 8667

Synthesis and alkaline stability of Aquivion-based perfluorinated anion exchange membranes

Li-Cheng Jheng, *[a] Yu-Hsiang Tsai,[a] Tai-Hai Huang,[a] Pin-Shen Lin,[a] Chen-Yu Chen, [bc] Chun-Jern Pan [a] and Che-Yi Chu [d]

Quaternized perfluorinated polymers are promising anion exchange membranes (AEMs) for hydrogen energy devices due to their excellent dimensional stability and high ionic conductivity, which arise from limited ion exchange capacities (IECs) and well-developed hydrophilic/hydrophobic microphase-separated morphologies. However, their poor alkaline stability remains a critical challenge. In this study, a series of Aquivion-based perfluorinated AEMs was synthesized with varied tethering structures to systematically examine the effects of sulfonyl-containing linkages, alkyl spacers, and nitrogen-based cyclic cationic end groups on alkaline stability. We specifically introduced sulfonate ester linkages and alkaline-stable cationic groups, such as *N*-methylpiperidinium and 1,2-dimethylimidazolium, into perfluorinated AEMs, as these functionalities have not been previously used in such systems. Compared with the sulfonyl- and sulfonate ester-linked AEMs, the sulfonamide-linked AEMs incorporating hexyl spacers exhibited markedly enhanced alkaline stability by preventing hydrolytic cleavage of the linkage between the perfluoroalkyl ether side chains and cationic end groups. Among them, the AEM bearing *N*-methylpiperidinium end groups (Aquivion-SO_2NH-6CPip) showed greater hydroxide conductivity retention (83.8%) after immersion in 1 M KOH at 60 °C for 192 h, while the AEM containing 1,2-dimethylimidazolium end groups (Aquivion-SO_2NH-6CIm) achieved a higher hydroxide conductivity of 2.56×10^{-2} S cm^{-1} at 80 °C. Both Aquivion-SO_2NH-6CIm and Aquivion-SO_2NH-6CPip demonstrated good potential in water electrolysis and fuel cell applications. Notably, the Aquivion-SO_2NH-6CIm AEM exhibited good water electrolysis performance, achieving a high current density of 518 mA cm^{-2} at 2.2 V, which is comparable to that of the commercial Sustainion X37-RT membrane.

Received 9th December 2025
Accepted 5th February 2026

DOI: 10.1039/d5ra09534d

rsc.li/rsc-advances

1. Introduction

Hydrogen is a sustainable fuel produced through water electrolysis powered by renewable energy and converted into clean electricity in fuel cells without carbon emission.[1–3] A proton exchange membrane (PEM), a key component of both fuel cells and water electrolyzers, significantly impacts the performance and durability of these hydrogen energy devices.[4,5] Among the various types of PEMs, perfluorinated PEMs comprising a polytetrafluoroethylene (PTFE) backbone with perfluoroalkyl ether side chains terminated by sulfonic acid groups, namely perfluorosulfonic acid (PFSA), have been widely adopted as the standard material, such as Nafion®, 3M™, and Aquivion® ionomer membranes.[6–9] Perfluorinated PEMs are distinguished by (i) excellent proton conductivity combined with balanced dimensional stability, arising from their well-defined hydrophilic/hydrophobic microphase-separated morphology containing interconnected ionic clusters and water channels, (ii) exceptional chemical stability, owing to the fully fluorinated polymer backbone, and (iii) good mechanical properties, conferred by their semicrystalline structure and relatively low ion exchange capacity (IEC).[10–12]

In recent decades, there has been growing focus on operating fuel cells and water electrolyzers under alkaline conditions using anion exchange membranes (AEMs) with non-precious metal catalysts, since this method provides a cost-effective alternative to acidic PEM-based systems that depend on expensive noble metal catalysts.[13–16] However, most AEMs intrinsically exhibit lower ionic conductivity than PEMs because hydroxide ions have lower mobility than protons.[17] In addition, AEMs face a trade-off between ionic conductivity and dimensional stability, as increasing IEC boosts ionic conductivity but also results in higher water uptake (WU) and swelling ratio (SR).[18] To address this trade-off, an effective strategy involves designing AEMs with comparatively low IECs, complemented by well-developed hydrophilic/hydrophobic microphase-separated

[a]*Department of Chemical and Materials Engineering, National Kaohsiung University of Science and Technology, Kaohsiung 80778, Taiwan. E-mail: lcjheng@nkust.edu.tw; Fax: +886 7 3830674; Tel: +886 7 3814526 ext.15148*

[b]*Graduate Institute of Energy Engineering, National Central University, Taoyuan 32001, Taiwan*

[c]*Department of Mechanical Engineering, National Central University, Taoyuan 32001, Taiwan*

[d]*Department of Chemical Engineering, National Chung Hsing University, Taichung 40227, Taiwan*

morphologies that facilitate ion transport while constraining swelling.[19] In this context, quaternized perfluorinated polymers have attracted significant interest as AEMs because their extremely hydrophobic backbones and hydrophilic cationic side chains readily promote such morphologies.[20–23] Consequently, unlike hydrocarbon-based AEMs, perfluorinated AEMs do not necessarily require additional modifications such as cross-linking or porous support reinforcement, which are commonly employed to balance membrane properties.[24]

However, perfluorinated AEMs typically show limited alkaline stability, especially when their strongly electron-withdrawing perfluoroalkyl ether side chains are directly attached to electron-deficient cationic end groups, making them highly susceptible to hydroxide attack through nucleophilic substitution.[25–27] Bosnjakovic *et al.* reported that quaternized perfluorinated polymers, prepared by reacting a 3M-based sulfonyl fluoride precursor with various tertiary amines, hydrolyze into acidic sulfonated perfluorinated PEMs rather than remaining as AEMs when exposed to 1 M KOH.[28] Recently, Lee and colleagues observed a similar instability in perfluorinated AEMs derived from Nafion- or Aquivion-based sulfonyl fluoride precursors, where the sulfonyl ammonium groups hydrolyzed to sulfonic acids after 96 hours in 0.5 M NaOH.[29] Fortunately, it is possible to improve the alkaline stability of perfluorinated AEMs by introducing an appropriate spacer between the perfluoroalkyl ether side chains and the cationic end groups through a chemically stable linkage. For example, Kim and co-workers reported that Nafion-based perfluorinated anion exchange ionomers containing pentamethylguanidinium groups exhibited good alkaline stability when the sulfonyl linkage was replaced with an amide linkage and a phenyl spacer was used introduced.[26] Park and co-workers created an alkaline-stable perfluorinated AEM by attaching trimethylammonium cations to a 3M-based sulfonyl fluoride precursor through a hexyl spacer and a sulfonamide linkage.[30] Similarly, Liu and co-workers demonstrated that incorporating aliphatic spacers can effectively stabilize short-side-chain perfluorinated AEMs, leading to improved alkaline stability.[31–33]

Another reason why perfluorinated AEMs have gained significant interest is that they can be synthesized from mass-produced perfluorinated sulfonyl fluoride precursors originally created for perfluorinated PEMs, providing an advantage for potential commercialization.[34] Here, we report the synthesis of a series of Aquivion-based perfluorinated AEMs with different combinations of linkages, spacers, and cationic end groups using various synthetic routes. The effect of tethering structures on the alkaline stability of Aquivion-based perfluorinated AEMs was systematically studied, with particular emphasis on the cleavage of sulfonyl-containing linkages (*e.g.*, sulfonyl, sulfonate ester, and sulfonamide) under alkaline hydrolysis conditions. As mentioned earlier, previous studies have demonstrated that introducing appropriate alkyl spacers can enhance the alkaline stability of perfluorinated AEMs. However, alkaline-stable nitrogen-based cyclic cations, such as 1,2-dimethylimidazolium and *N*-methylpiperidinium, which are widely used in hydrocarbon-based AEMs,[35–39] have not yet been incorporated into perfluorinated AEM systems. Therefore, in this work, we specifically synthesized Aquivion-based perfluorinated AEMs containing *N*-methylpiperidinium and 1,2-dimethylimidazolium cationic groups to investigate their effects on alkaline stability. The membrane properties of the Aquivion-based perfluorinated AEMs were also studied, and their potential for hydrogen energy applications was evaluated through anion exchange membrane water electrolysis (AEMWE) and anion exchange membrane fuel cell (AEMFC) tests.

2. Experimental

2.1. Materials

All reagents were used without further purification and are listed as follows: 2-bromoethoxy-*tert*-butyldimethylsilane (99%, Sigma-Aldrich), 1,2-dimethylimidazole (96%, Thermo Scientific), 1,6-dibromohexane (97%, Alfa Aesar), *N*-methylpiperidine (99%, Sigma-Aldrich), 1,8-diazabicyclo[5.4.0]undec-7-ene (DBU) (98%, Sigma-Aldrich), *N*,*N*-diisopropylethylamine (Hünig's base) (99.5%, Sigma-Aldrich), ammonium hydroxide (30 wt%, J.T. Baker), potassium hydroxide (85%, Acros Organics), potassium bromide (99%, Alfa Aesar), silver nitrate (99.85%, Acros Organics), and sodium nitrate (99%, Showa). The solvents used in this study for synthesis and characterization were as follows: dimethylformamide (DMF) (99.8%, Thermo Scientific), dimethyl sulfoxide (DMSO) (99.9%, Acros Organics), methanol (99%, Macron Fine Chemicals™), diethyl ether (99.8%, Honeywell Fluka™), acetonitrile (99.6%, Acros Organics), and deuterated dimethyl sulfoxide-d_6 (DMSO-d_6) (99.9%, Sigma-Aldrich). The Aquivion-based perfluorinated sulfonyl fluoride precursor pellets (Aquivion® P87S-SO_2F with an equivalent weight of 870 g mol^{-1}, Solvay) were purchased from the Fuel Cell Store.

2.2. Synthesis of a perfluorinated sulfonamide precursor (Aquivion-SO_2NH_2)

Perfluorinated sulfonyl fluoride precursor (Aquivion-SO_2F) (10 mmol), ammonium hydroxide (45 mmol), and DMF (80 g) were stirred with a magnetic stirrer. After 30 days of stirring, the precursor pellets were fully dissolved, forming a clear solution. The solution was then heated to 100 °C with stirring for 2 h to remove residual ammonia, then poured into deionized water, which precipitated a light brown polymer powder. The precipitate was washed with methanol and diethyl ether to remove residual solvents and impurities. After drying, the brown powder of perfluorinated sulfonamide precursor (Aquivion-SO_2NH_2) was obtained.

2.3. Synthesis of cationic compounds (TBS-2CIm, Br-6CIm, and Br-6CPip)

2-Bromoethoxy-*tert*-butyldimethylsilane (6.5 mmol) was dissolved in 10 mL of acetonitrile under magnetic stirring and a nitrogen atmosphere at 60 °C. Subsequently, 6 mmol of 1,2-dimethylimidazole was added to the solution, and the Menshutkin reaction was conducted at 60 °C for 12 h. After the reaction, the mixture was cooled to room temperature and poured into excess diethyl ether to precipitate a viscous product and remove unreacted compounds. The collected product was then dried

under magnetic stirring and reduced pressure at 90 °C overnight. Finally, the 1,2-dimethylimidazolium cationic compound with an ethoxy butyldimethylsilane group, named TBS-2CIm, was obtained. 18 mmol of 1,6-dibromohexane and 50 mL of acetonitrile were stirred magnetically at 60 °C. A solution of 1,2-dimethylimidazole (15 mmol) in 30 mL of acetonitrile was then added dropwise *via* a dropping funnel to the mixture, allowing the Menshutkin reaction to proceed for 12 hours. After cooling to room temperature, the mixture was poured into a 500 mL beaker containing excess diethyl ether to precipitate a viscous liquid at the bottom and remove unreacted 1,6-dibromohexane. The residual solvent in the collected liquid was evaporated under reduced pressure at 90 °C with stirring. The resulting 1,2-dimethylimidazolium cationic compound with a hexyl bromide group, named Br-6CIm, was obtained. The synthesis of the *N*-methylpiperidinium cationic compound with a hexyl bromide group, called Br-6CPip, is similar to that of Br-6CIm, except that 1,2-dimethylimidazole is replaced by *N*-methylpiperidine.

2.4. Synthesis of sulfonyl-linked 1,2-dimethylimidazolium perfluorinated anion exchange membranes (Aquivion-SO_2N-Im)

Aquivion-SO_2F (5 mmol) was reacted with 1,2-dimethylimidazole (7.5 mmol) *via* the Menshutkin reaction at 150 °C in anhydrous DMAc (150 mL) for 12 h. During the reaction, the Aquivion-SO_2F particles gradually dissolved in the solution as they were converted into a sulfonyl-linked 1,2-dimethylimidazolium perfluorinated polymer, denoted as Aquivion-SO_2N-Im. The polymer was then precipitated using excess diethyl ether, washed three times with diethyl ether, and dried under vacuum at 90 °C, yielding a beige powder of Aquivion-SO_2N-Im. Aquivion-SO_2N-Im AEMs were fabricated *via* a solvent casting process, which involved preparing a 5 wt% polymer solution, solidifying it at 120 °C under vacuum for 12 h, washing with methanol, and drying in an 80 °C air-flow oven.

2.5. Synthesis of sulfonate ester-linked ethyl 1,2-dimethylimidazolium perfluorinated anion exchange membranes (Aquivion-SO_3-2CIm)

Aquivion-SO_2F (5 mmol) was reacted with the cationic compound TBS-2CIm (15 mmol) in anhydrous DMAc (150 mL) at 120 °C for 12 h *via* the sulfur(VI) fluoride exchange (SuFEx) reaction, using DBU as a catalyst. After cooling to room temperature, the solution was poured into excess diethyl ether to precipitate the sulfonate ester-linked ethyl 1,2-dimethylimidazolium perfluorinated polymer, designated as Aquivion-SO_3-2CIm. The resulting polymer was purified by washing three times with diethyl ether and methanol. Finally, after vacuum drying at 90 °C, a beige powder of Aquivion-SO_3-2CIm was obtained. The membrane preparation of Aquivion-SO_3-2CIm AEMs follows the solvent casting described previously.

2.6. Synthesis of sulfonamide-linked hexyl 1,2-dimethylimidazolium perfluorinated anion exchange membranes (Aquivion-SO_2NH-6CIm)

A sulfonamide-linked hexyl 1,2-dimethylimidazolium perfluorinated polymer, denoted as Aquivion-SO_2NH-6CIm, was synthesized by reacting Br-6CIm (15.0 mmol) with the precursor Aquivion-SO_2NH_2 (5.0 mmol) in the presence of Hünig's base (5.0 mmol) at 120 °C for 24 h using anhydrous DMAc as the solvent. After the reaction, the solution was cast onto a glass plate and heated at 120 °C for 12 h to form a membrane. The membrane was then peeled off by immersion in deionized water and subsequently washed with methanol to remove residual solvent and unreacted compounds. After drying in an 80 °C air-flow oven, the Aquivion-SO_2NH-6CIm AEM was obtained.

2.7. Synthesis of sulfonamide-linked hexyl *N*-methylpiperidinium perfluorinated anion exchange membranes (Aquivion-SO_2NH-6CPip)

A sulfonamide-linked hexyl *N*-methylpiperidinium perfluorinated polymer, referred to as Aquivion-SO_2NH-6CPip, was synthesized by reacting Br-6CPip (15.0 mmol) with the precursor Aquivion-SO_2NH_2 (5.0 mmol) in the presence of Hünig's base (5.0 mmol) at 120 °C for 24 h using anhydrous DMAc as the solvent. The subsequent procedure for preparing the Aquivion-SO_2NH-6CPip AEMs is identical to that of the Aquivion-SO_2NH-6CIm AEMs.

2.8. Characterization

Fourier transform infrared (FTIR) spectroscopy was performed using a PerkinElmer Spectrum ONE instrument. Liquid-state nuclear magnetic resonance (NMR) analysis was conducted on a Bruker AVANCE III HD 600 MHz spectrometer for samples dissolved in DMSO-d_6. X-ray photoelectron spectroscopy (XPS) was conducted with a ULVAC-PHI PHI 5000 VersaProbe utilizing a monochromatic Al Kα radiation source (1486.6 eV). Thermogravimetric analysis (TGA) was performed using a TA/SDT-Q600 instrument at a heating rate of 10 °C min^{-1} from 100 °C to 800 °C under a nitrogen flow of 100 mL min^{-1}. Small-angle X-ray scattering (SAXS) data were collected using the In-vacuum Eiger X 9M detector at the 25A beamline of the Taiwan Photon Source (TPS). Atomic force microscopy (AFM) phase images of the AEM samples were obtained in tapping mode using a Bruker Dimension ICON SPM instrument at ambient temperature. Transmission electron microscopy (TEM) images were acquired using a JEOL JEM-2100F instrument at an accelerating voltage of 120 kV for AEMs stained with RuO_4. The water contact angle (WCA) and oil contact angle (OCA) of the membrane surfaces were measured using a contact angle analyzer (OSA60SS, LAUDA) to evaluate their surface wettability. Deionized water and dodecane were used as the probe liquids for WCA and OCA measurements, and the droplet volume was fixed at 20 μL.

2.9. Measurements of membrane properties

The actual ion exchange capacity (IEC) was determined by Morh's titration. An AEM in the Cl^- ion form was immersed in 1 M Na_2SO_4 solution at room temperature for 24 h to facilitate the complete exchange of Cl^- ions into the solution. Then, the solution was titration with $AgNO_3$ aqueous solution, using K_2CrO_4 as a colorimetric indicator. The actual IEC can be calculated based on the consumed volume of $AgNO_3$ solution (V_{AgNO_3}), the $AgNO_3$ solution concentration (C_{AgNO_3}), and the dry membrane weight (m_{dry}) using the following equation:

$$\mathrm{IEC} = \frac{V_{\mathrm{AgNO_3}} \times C_{\mathrm{AgNO_3}}}{m_{\mathrm{dry}}}$$

Prior to measuring water uptake (WU) and swelling ratio (SR), the AEM in its Cl^- ion form was soaked in deionized water at 30 °C for 24 h. After gently wiping the membrane to remove surface water, its weight and length in the hydrated state (W_h and L_h) were recorded. The membrane was then dried in a vacuum oven at 100 °C for 4 h, followed by measuring its weight and length in the dry state (W_d and L_d). The WU and SR were calculated using the following equations:

$$\mathrm{WU}(\%) = \frac{W_h - W_d}{W_d} \times 100\%$$

$$\mathrm{SR}(\%) = \frac{L_h - L_d}{L_d} \times 100\%$$

The hydration number, representing the number of water molecules per cationic group in the AEM, was calculated using the IEC, WU, and the molar mass of water (18.02 g mol^{-1}) as shown below.

$$\lambda = \frac{\mathrm{WU} \times 1000}{\mathrm{IEC} \times 18.02}$$

The ionic conductivity (σ) of an anion exchange membrane was measured using a Metrohm Multi Autolab/M204 instrument with a two-probe cell immersed in N_2-saturated deionized water at a predetermined temperature in a sealed flask. Frequency response analysis (FRA) in the potentiostatic mode was performed over a frequency range of 10 kHz to 0.1 Hz to obtain the Nyquist plot. The ionic conductivity (σ) can be determined by the real impedance-axis intercept value (R_Ω), the membrane thickness (T), and the contact area (A) as follows.

$$\sigma = \frac{T}{R_\Omega \times A}$$

The effective ion mobility (μ) in an anion exchange membrane can be calculated using ionic conductivity (σ), Faraday's constant (F), and ion concentration (n). According to P. Knauth's method, the ion concentration (n) in an anion exchange membrane can be determined by IEC and WU, which is directly related to the hydration number (λ).[40] The following equations are used to calculate effective ion mobility (μ).

$$\mu = \frac{\sigma}{F \times n}$$

$$n = \frac{\mathrm{IEC}}{\mathrm{WU}} = \frac{1000}{\lambda \times 18.02}$$

The mechanical properties of the AEM samples were evaluated using a Shimadzu AG-SI universal testing machine under ambient conditions. Membrane specimens were cut into strips with dimensions of 50 mm × 4.5 mm and tested at a stretching speed of 20 mm min^{-1}. At least six specimens were measured for each sample, and the reported values of elastic modulus, tensile strength, and strain at break represent the averaged results.

2.10. Water electrolysis and fuel cell tests

The water electrolysis test was performed using a zero-gap cell (5 cm^2 electrolyzer hardware, Dioxide Materials) controlled by a potentiostat/galvanostat (Autolab PGSTAT204, Metrohm) equipped with a current booster (BOOSTER10A, Metrohm) for power supply, monitoring, and data acquisition. Prior to testing, the zero-gap cell containing an AEM was conditioned by circulating 1 M KOH at 60 °C and a flow rate of 25 mL min^{-1} under a constant voltage of 1.5 V for 15 min. Subsequently, the polarization curve was recorded in potentiostatic mode by scanning the cell voltage from 1.2 V to 2.2 V in 0.05 V increments. Ni foam and NiFe catalyst-coated Ni foam were employed as electrodes in the zero-gap cell. The preparation procedure for the NiFe catalyst-coated Ni foam electrodes is described in detail in SI.

The fuel cell test was conducted using a single cell operated on a fuel cell testing system (Tension Energy, Inc., Taiwan) equipped with an electronic load controller. The single cell, with an active area of 4 cm^2, consisted of a membrane electrode assembly (MEA) fabricated by sandwiching an AEM between two gas diffusion electrodes (GDEs) without hot pressing. During operation, humidified hydrogen and oxygen gases (60 °C, 100 mL min^{-1}) were supplied to the anode and cathode, respectively, without applying backpressure. After the open-circuit voltage (OCV) stabilized, the polarization curve was recorded in potentiostatic mode by decreasing the cell voltage from the OCV to 0.2 V. The procedure for preparing GDEs is described in detail in Supplementary Information.

3. Results and discussion

3.1. Synthesis and characterization of cationic compounds and Aquivion-based perfluorinated anion exchange membranes

In this study, we synthesized a series of Aquivion-based perfluorinated AEMs with varying linkages, spacers, and cationic end groups, including Aquivion-SO_2N-Im, Aquivion-SO_3-2CIm, Aquivion-SO_2NH-6CIm, and Aquivion-SO_2NH-6CPip, using SuFEx, Menshutkin, and S_N2 reactions. The SuFEx reaction generally involves the reaction of a sulfonyl fluoride with a silyl ether to form a sulfonate ester. The Menshutkin reaction specifically refers to the conversion of a tertiary amine into a quaternary ammonium salt by reaction with an alkyl halide. The synthetic routes are shown in Scheme 1.

Aquivion-SO_2N-Im is a sulfonyl-linked 1,2-dimethylimidazolium perfluorinated polymer without a spacer, while Aquivion-SO_3-2CIm features a sulfonate ester linkage and an ethyl spacer connected to a 1,2-dimethylimidazolium end group. Both polymers were derived from the perfluorinated sulfonyl fluoride precursor (Aquivion-SO_2F). Notably, Aquivion-SO_3-2CIm was obtained *via* a SuFEx reaction by reacting the *tert*-

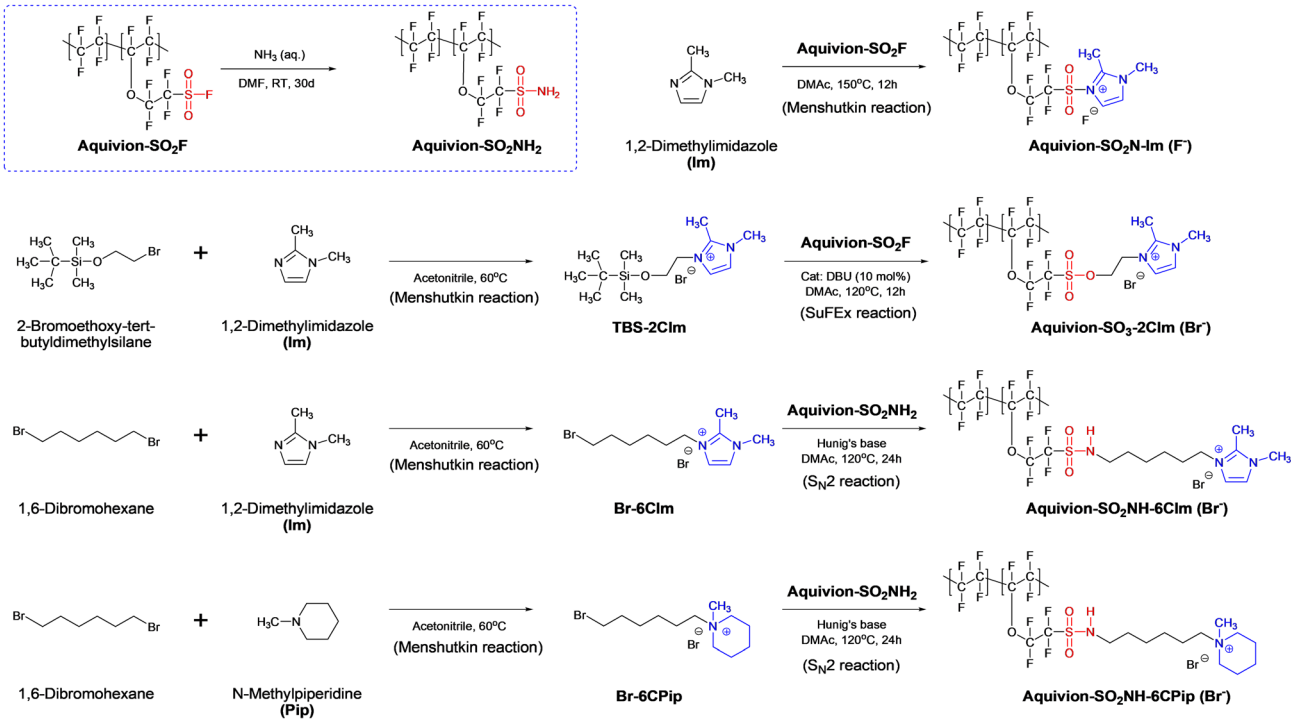

Scheme 1 Synthesis routes of cationic compounds and Aquivion-based perfluorinated anion exchange membranes.

butyldimethylsilyl ether group of TBS-2CIm cationic compound with the sulfonyl fluoride group of Aquivion-SO_2F.[41] In contrast, Aquivion-SO_2NH-6CIm and Aquivion-SO_2NH-6CPip were synthesized from the perfluorinated sulfonamide precursor (Aquivion-SO_2NH_2) by the nucleophilic substitution (S_N2) reaction with Br-6CIm and Br-6CPip cationic compounds, respectively, yielding sulfonamide-linked perfluorinated polymers with a hexyl spacer and 1,2-dimethylimidazolium or *N*-methylpiperidinium end groups. In addition, the precursor Aquivion-SO_2NH_2 was prepared by reacting solid Aquivion-SO_2F pellets with aqueous ammonia in DMF under heterogeneous conditions. The reaction was performed for 30 days to ensure the complete dissolution of the Aquivion-SO_2F pellets in the resulting solution.

The functional groups of cationic compounds and Aquivion-based perfluorinated polymers were analyzed by FTIR. The twin peaks corresponding to C–H asymmetric and symmetric stretching vibrations, observed at 2950–2930 cm^{-1} and 2865–2855 cm^{-1} in Fig. 1a, are attributed to the methyl and methylene groups in TBS-2CIm, Br-6CIm, and Br-6CPip.[42,43] The C=N stretching peak, originally located at 1529 cm^{-1} for the imidazole ring in dimethylimidazole (Im),[44] shifted to 1536 cm^{-1} and 1540 cm^{-1} for the imidazolium moiety in TBS-2CIm and Br-6CIm,[45,46] respectively, indicating successful quaternization. Additionally, the Si–C bond in TBS-2CIm and the C–N^+ bond in Br-6CPip were confirmed by the characteristic peaks at 1260 cm^{-1} and 945 cm^{-1}, respectively.[42,46]

In the FTIR spectra of all Aquivion-based perfluorinated polymers (Fig. 1b), an intense absorption band between 1300 and 1100 cm^{-1}, attributed to the C–F stretching vibrations of the polymer backbone, was observed.[32,47] The precursor Aquivion-SO_2F exhibited two peaks at 823 and 796 cm^{-1}, corresponding to the S–F stretching vibration.[32,48] Upon replacement of the S–F bond in Aquivion-SO_2F with the S–N bond in Aquivion-SO_2NH_2, the asymmetric SO_2 stretching peak was expected to shift from 1470 cm^{-1} to 1392 cm^{-1}.[31,32,48] However, we observed that the peaks associated with the SO_2F group at 1470, 823, and 796 cm^{-1} decreased markedly in intensity but still existed in the spectrum of Aquivion-SO_2NH_2. This suggests that the amination reaction of Aquivion-SO_2F to form Aquivion-SO_2NH_2 was not complete even after 30 days of reaction time. After coupling the side chains of perfluorinated precursors with Im, TBS-2CIm, Br-6CIm, and Br-6CPip compounds, the symmetric SO_2 stretching peaks associated with sulfonyl, sulfonamide, or sulfonate ester linkages appeared at 1051 cm^{-1} for Aquivion-SO_2N-Im and Aquivion-SO_3-2CIm, and at 1054 cm^{-1} for Aquivion-SO_2NH-6CIm and Aquivion-SO_2NH-6CPip.[43,49] In addition, the absorption bands corresponding to the C–H bond of the alkyl spacer (2950–2930 cm^{-1} and 2865–2855 cm^{-1}), the C=N bond of the imidazolium end-group (1536–1540 cm^{-1}), and the C–N^+ bond of the piperidinium end-group (945 cm^{-1}) were observed in the spectra of these Aquivion-based perfluorinated AEMs, as expected.

Fig. 2 shows the ^1H NMR spectra of cationic compounds and Aquivion-based perfluorinated AEMs. The methyl protons in 1,2-dimethylimidazole (Im), assigned to signals at 2.23 ppm and 3.51 ppm (denoted as H_a and H_b), shifted to 2.58 ppm and 3.77 ppm after quaternization of Im to form TBS-6CIm and Br-6Im cationic compounds. Meanwhile, the imidazole proton signals originally observed at 6.67 ppm (H_c) and 6.96 ppm (H_d) for Im shifted to 7.61–7.63 ppm for TBS-6CIm as well as 7.64–7.70 ppm for Br-6CIm. Similar shifts of these proton signals (H_a,

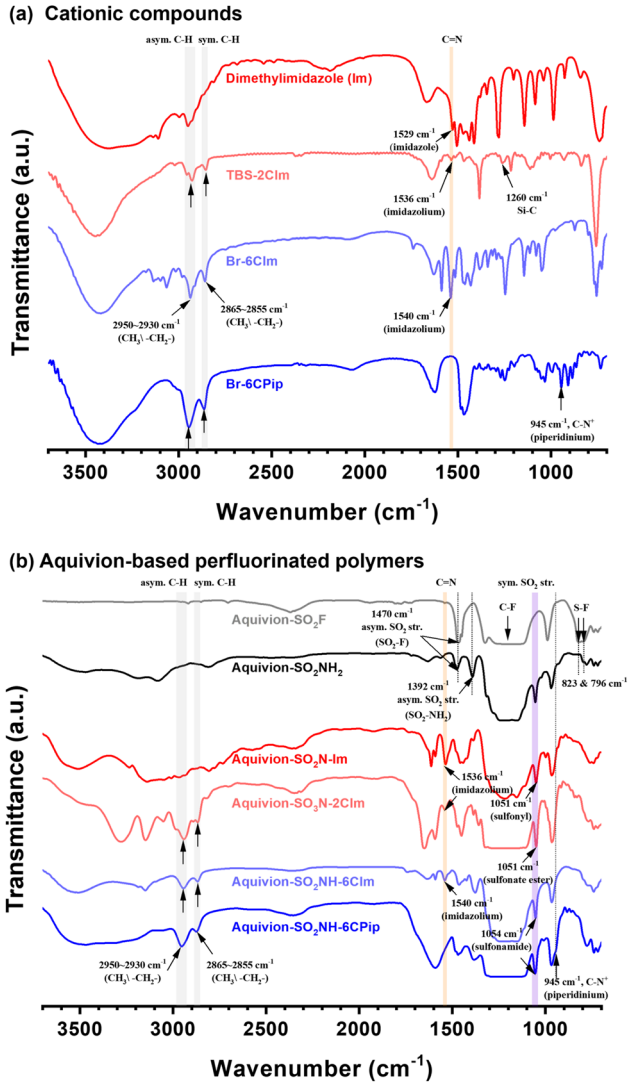

Fig. 1 FTIR spectra of (a) the cationic compounds (Im, TBS-2CIm, Br-6CIm, and Br-6CPip) as well as (b) the Aquivion-based perfluorinated AEMs and their precursors.

H_b, H_c, and H_d) were also observed when Im was coupled with Aquivion-SO_2F to form Aquivion-SO_2N-Im. In addition, the methyl proton signals of the *tert*-butyldimethylsilyl group in TBS-2CIm at −0.06 ppm (H_w) and 0.79 ppm (H_x) disappeared, while the methylene proton signals associated with the ethyl spacer were retained but slightly shifted from 3.86 ppm (H_y) and 4.25 ppm (H_z) to 3.67 ppm and 4.15 ppm, respectively, confirming the successful synthesis of Aquivion-SO_3-2CIm.

For Br-6CIm and Br-6CPip, the methylene proton signals were distributed between 1.2 and 4.1 ppm. Among these, the signals from methylene protons adjacent to nitrogen appeared at 4.11 ppm for Br-6CIm and at 3.28–3.53 ppm for Br-6CPip.[50,51] The individual methylene proton assignments of Br-6CPip were confirmed by its COSY spectrum (Fig. S1). When hexyl dimethylimidazolium and hexyl methylpiperidinium were tethered to perfluorinated polymer *via* a sulfonamide linkage to yield Aquivion-SO_2NH-6CIm and Aquivion-SO_2NH-6CPip, a signal near 7.1 ppm, attributable to the SO_2NH proton, was observed (Fig. 2b). However, its intensity was fairly weak, likely due to zwitterionic behavior of the sulfonamide group interacting with the cationic end groups (Fig. S2).[30,52] Aside from this, the proton signals corresponding to the hexyl dimethylimidazolium and hexyl methylpiperidinium groups in Aquivion-SO_2NH-6CIm and Aquivion-SO_2NH-6CPip were present and slightly shifted upfield. In addition, XPS analysis was used to detect elements in Aquivion-based perfluorinated AEMs. As shown in Fig. S3, characteristic peaks for S 2p (∼168 eV), C 1s (∼291 eV), N 1s (∼400 eV), O 1s (∼532 eV), and F 1s (∼688 eV) appeared as expected. The combined FTIR, ^{1}H NMR, and XPS results confirm the successful synthesis of the cationic compounds and Aquivion-based perfluorinated AEMs.

3.2. Physicochemical properties of Aquivion-based perfluorinated anion exchange membranes

The degree of functionalization (DF) of the Aquivion-based perfluorinated AEMs was estimated from the ratio of the theoretical IEC to the measured IEC, as listed in Table 1. For the Aquivion-SO_2N-Im and Aquivion-SO_3-2CIm AEMs, their DF values were determined to be 88.2% and 81.8%, respectively, which are comparable to those of other perfluorinated AEMs (75–85%) reported previously.[30] In contrast, the Aquivion-SO_2NH-6CIm and Aquivion-SO_2NH-6CPip AEMs, prepared from the precursor Aquivion-SO_2NH_2, exhibited relatively lower DF values (31.9% and 28.9%), primarily due to incomplete amination of their precursor as mentioned earlier in the FTIR result.

Water uptake (WU), swelling ratio (SR), and hydration number (λ) reflect the membrane's dimensional stability and its ability to promote microphase separation, both of which are crucial for the performance of AEMs in electrochemical devices such as fuel cells and water electrolyzers. Owing to the ultrahydrophobic polytetrafluoroethylene backbone and limited IEC, the Aquivion-based perfluorinated AEMs synthesized in this study exhibited low WU values of 4.0–14.1 wt% and low SR values of 5.8–8.1%, both considerably lower than those of most commercially available AEMs.[53] The hydration number λ, calculated as the ratio of WU to IEC, represents the number of water molecules associated with each cationic group in the AEM. Interestingly, regardless of IEC and DF, the three AEMs bearing 1,2-dimethylimidazolium cations (Aquivion-SO_2N-Im, Aquivion-SO_3-2CIm, and Aquivion-SO_2NH-6CIm) exhibited nearly identical λ values (8.7–8.8), whereas the Aquivion-SO_2NH-6CPip AEM carrying *N*-methylpiperidinium cations had a lower λ value of 6.3. This result highlights the critical influence of cation type on hydrophilic/hydrophobic microphase separation in perfluorinated membranes and implies that 1,2-dimethylimidazolium cations may have better affinity with water molecules than *N*-methylpiperidinium cations.

The surface wettability of the Aquivion-based perfluorinated AEMs was evaluated by measuring the water contact angle (WCA) and oil contact angle (OCA). As shown in Fig. S4, these AEMs exhibited hydrophobic and oleophilic surface characteristics, with WCAs ranging from 99.6° to 108.1° and OCAs below

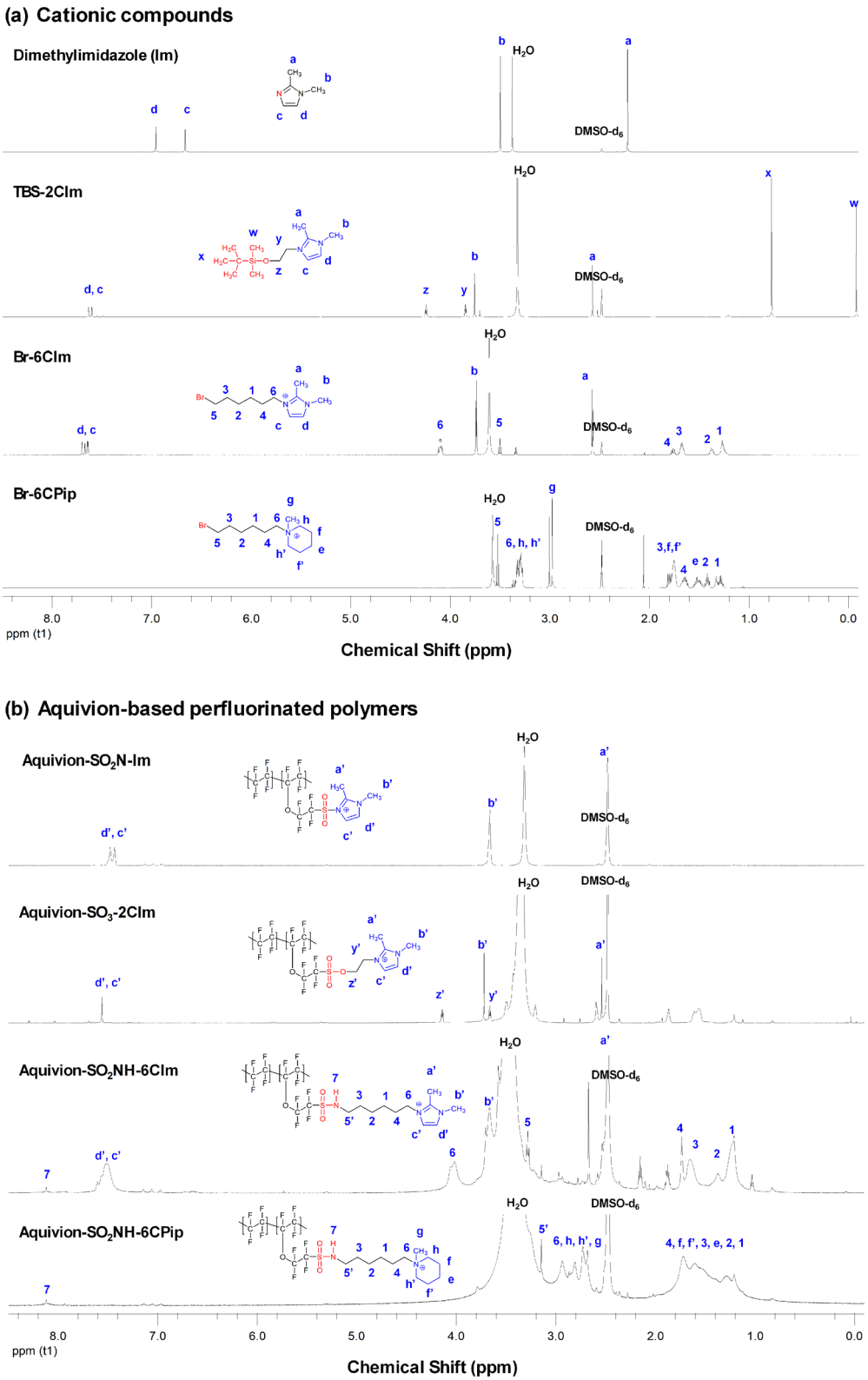

Fig. 2 ^{1}H NMR spectra of (a) the cationic compounds (Im, TBS-2ClIm, Br-6ClIm, and Br-6CPip) as well as (b) the Aquivion-based perfluorinated AEMs.

Table 1 Ion exchange capacity, degree of functionalization, water uptake, swelling ratio, and hydration number of the Aquivion-based perfluorinated AEMs

Membrane code	Linkage	Spacer	Cation	IEC (mmol g^{-1})		DF[c] (%)	WU[d] (wt%)	SR[e] (%)	λ[f]
				Theoretical[a]	Measured[b]				
Aquivion-SO_2N-Im	Sulfonyl	None	1,2-Dimethylimidazolium	1.02	0.91	88.2	14.1	8.1	8.7
Aquivion-SO_3-2CIm	Sulfonate ester	Ethyl	1,2-Dimethylimidazolium	0.97	0.82	81.8	12.9	8.0	8.8
Aquivion-SO_2NH-6CIm	Sulfonamide	Hexyl	1,2-Dimethylimidazolium	0.93	0.34	31.9	5.1	6.8	8.7
Aquivion-SO_2NH-6CPip	Sulfonamide	Hexyl	*N*-Methylpiperidinium	0.92	0.31	28.9	4.0	5.8	6.3

[a] Theoretical ion exchange capacity (IEC) refers to the IEC of the AEM with the 100% degree of functionalization. [b] Measured ion exchange capacity (IEC) was obtained by titration for the AEM in Cl^- form. [c] Degree of functionalization (DF) is defined as the ratio of the number of cation end-group to a repeated unit. [d] Water uptake (WU) was determined by the weight difference between the AEM in fully hydrated state and in the dried state at 30 °C. [e] Swelling ratio (SR) was determined by the length difference between the AEM in fully hydrated state and in the dried state at 30 °C. [f] Hydration number (λ) is defined as the number of water molecules for each cation end-group.

16.6°. The hydrophobicity of these AEMs is similar to that of the Nafion proton exchange membrane (WCA = 105°) and slightly weaker than that of PTFE (Teflon) (WCA = 110°).[54]

3.3. Alkaline stability of Aquivion-based perfluorinated anion exchange membranes

Due to the strong electron-withdrawing effects of the perfluoroalkyl side chains and cationic end groups in the perfluorinated AEMs, the sulfonyl-containing linkages (such as sulfonyl, sulfonamide, and sulfonate ester) that connect these side chains to the cationic groups are highly vulnerable to nucleophilic attack by hydroxide ions, especially under strongly basic conditions. As a result, these linkages undergo alkaline hydrolysis, transforming into sulfonic acid groups.[28] As a result, the perfluorinated AEMs are transformed into perfluorinated PEMs (*i.e.*, perfluorosulfonic acid (PFSA) polymers).[55] Recently, Lee *et al.* reported that the alkaline hydrolysis of perfluorinated AEMs can be identified by the appearance of an FTIR absorption peak at 1060 cm^{-1}, corresponding to the symmetric SO_2 stretching of the sulfonic acid group.[48] This method enables a facile assessment of the alkaline hydrolysis of perfluorinated AEMs.

Fig. 3 compares the FTIR spectral evolutions of the Aquivion-based perfluorinated AEMs synthesized in this work under alkaline conditions. For Aquivion-SO_2N-Im, the absorption peak of the symmetric SO_2 stretching shifted from 1051 cm^{-1} to 1060 cm^{-1} after exposure to 0.2 M KOH at room temperature for 0.5 h, indicating that its sulfonyl linkage was hydrolyzed to form a sulfonic acid end group. In contrast, the Aquivion-SO_3-2CIm AEM underwent alkaline hydrolysis of the sulfonate ester linkage when immersed in 1 M KOH at room temperature for 1 h. On the other hand, no shift of the symmetric SO_2 stretching peaks was observed in the FTIR spectra of Aquivion-SO_2NH-6CIm and Aquivion-SO_2NH-6CPip, even after treatment in 1 M KOH at 60 °C for 192 h. Moreover, the absorption peaks corresponding to the C=N bond of the imidazolium group in Aquivion-SO_2NH-6CIm (1540 cm^{-1}) and the C–N^+ bond of the piperidinium group in Aquivion-SO_2NH-6CPip (945 cm^{-1}) remained intact after the prolonged alkaline treatment. In contrast, the C=N peak of imidazolium cations disappeared for Aquivion-SO_2N-Im and was only partially retained for Aquivion-SO_3-2CIm after alkaline treatment. These results demonstrate that Aquivion-SO_2N-Im is more susceptible to alkaline hydrolysis than Aquivion-SO_3-2CIm. However, both of them are much less alkaline stable than Aquivion-SO_2NH-6CIm and Aquivion-SO_2NH-6CPip.

We further employed TGA to investigate the thermogram changes of Aquivion-based perfluorinated AEMs under alkaline degradation conditions, aiming to gain a better understanding of their alkaline stability. As shown in Fig. 4, the thermograms of all Aquivion-based perfluorinated AEMs prior to alkaline treatment exhibited two distinct weight loss steps. The first weight loss step, observed between 350 °C and 420 °C, corresponds to the thermal decomposition of cationic end groups and alkyl spacers in the perfluorinated polymer, while the second weight loss step, occurring above 420 °C, is attributed to the decomposition of the remaining polymer backbone.[56] However, for both Aquivion-SO_2N-Im and Aquivion-SO_3-2CIm, after 1 h of alkaline treatment in 1 M KOH solution at room temperature, the weight-loss associated with the cationic groups and alkyl spacers completely disappeared, and only a single decomposition step at around 450 °C was observed. This result can be attributed to the alkaline hydrolysis of Aquivion-SO_2N-Im and Aquivion-SO_3-2CIm, which converts them into the PFSA polymer (Aquivion-SO_3H) with the loss of cationic end groups.

On the other hand, the thermograms of Aquivion-SO_2NH-6CIm and Aquivion-SO_2NH-6CPip still exhibited the 350–420 °C weight-loss step even after 192 h of alkaline treatment in 1 M KOH at 60 °C. This weight loss, attributed to the thermal decomposition of the cationic groups and alkyl spacers, was less pronounced for Aquivion-SO_2NH-6CIm (Fig. 4c) than for Aquivion-SO_2NH-6CPip (Fig. 4d). This observation suggests that a greater fraction of the hexyl 1,2-dimethylimidazolium units in Aquivion-SO_2NH-6CIm had already undergone alkaline degradation prior to thermal decomposition compared with the hexyl *N*-methylpiperidinium units in Aquivion-SO_2NH-6CPip. Accordingly, Aquivion-SO_2NH-6CPip exhibits higher alkaline stability than Aquivion-SO_2NH-6CIm.

Taken together, the TGA and FTIR results show that the alkaline stability of these AEMs follows the order: Aquivion-SO_2N-Im < Aquivion-SO_3-2CIm < Aquivion-SO_2NH-6CIm <

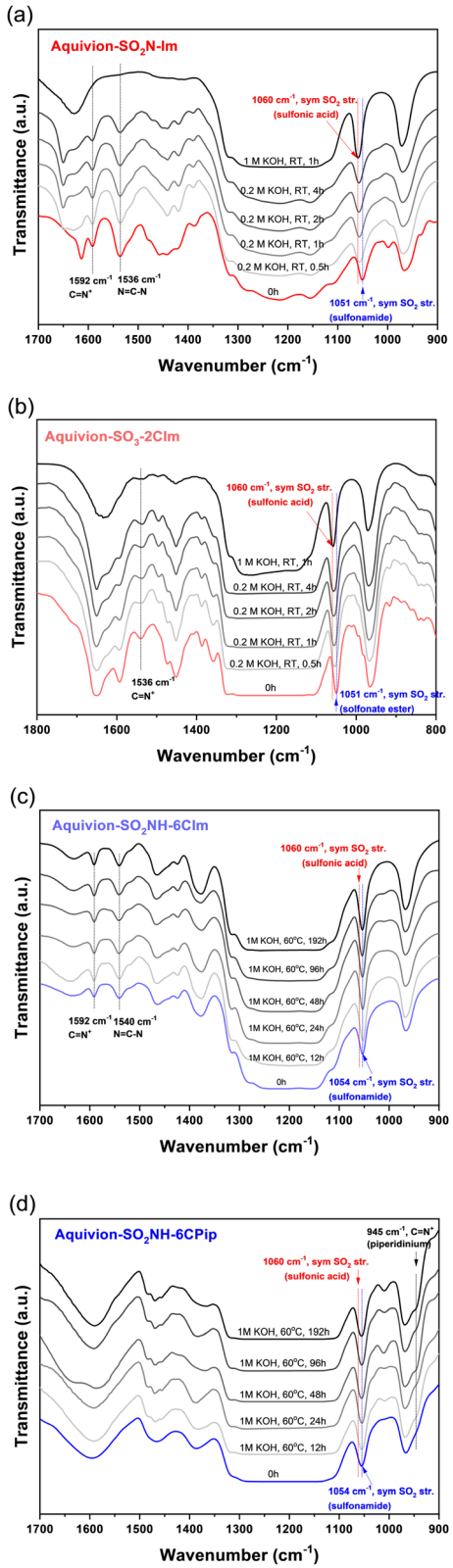

Fig. 3 FTIR spectral evolution of (a) Aquivion-SO_2N-Im, (b) Aquivion-SO_3-2ClIm, (c) Aquivion-SO_2NH-6ClIm, and (d) Aquivion-SO_2NH-6CPip during alkaline treatment.

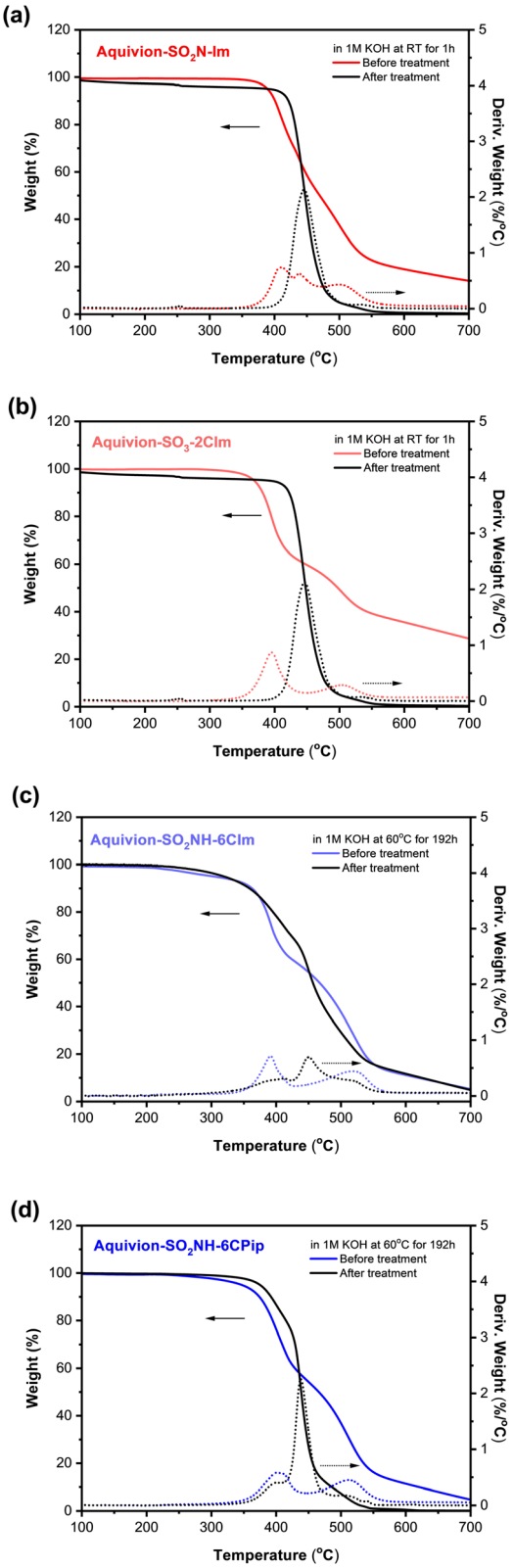

Fig. 4 Thermograms and derivative thermogravimetric (DTG) curves of (a) Aquivion-SO_2N-Im, (b) Aquivion-SO_3-2ClIm, (c) Aquivion-SO_2NH-6ClIm, and (d) Aquivion-SO_2NH-6CPip before and after alkaline treatment.

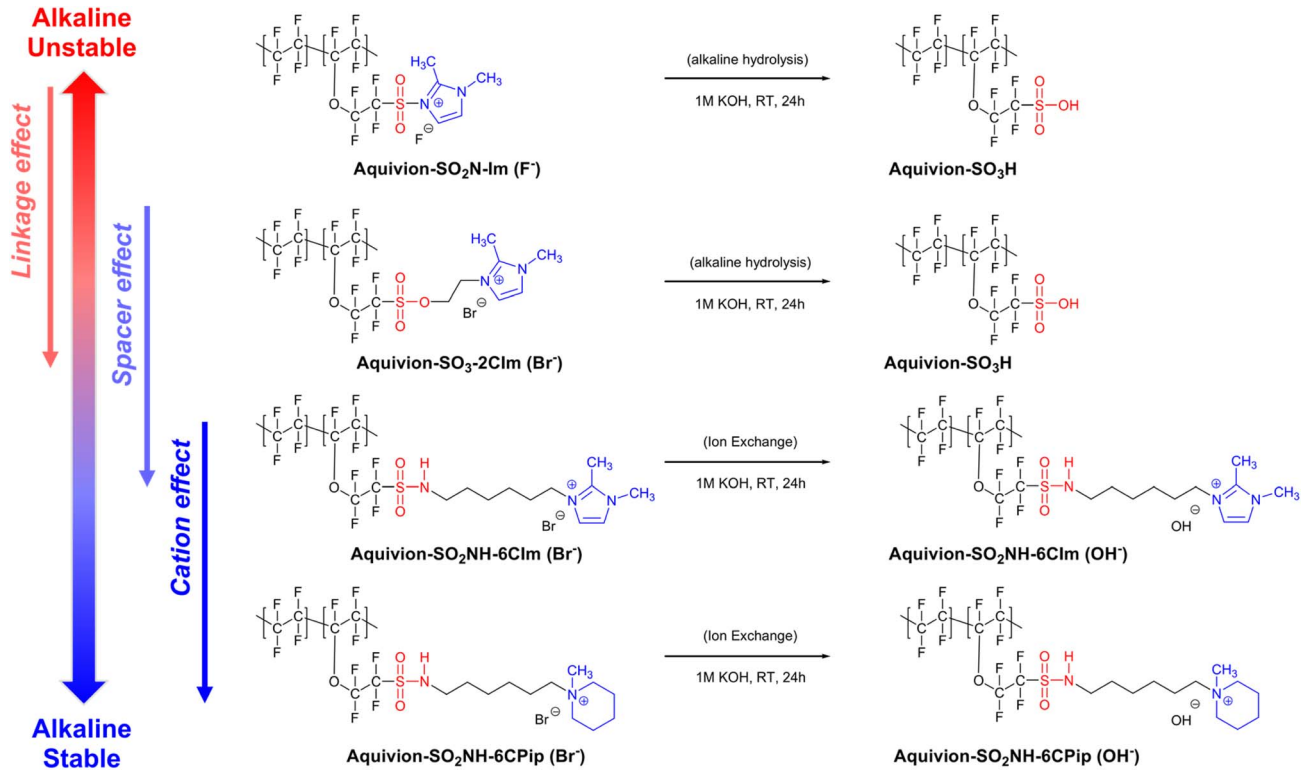

Scheme 2 Alkaline stability comparison of the Aquivion-based perfluorinated AEMs with various linkages, spacers, and cationic end groups.

Aquivion-SO_2NH-6CPip, as illustrated in Scheme 2. The alkaline instability of perfluorinated AEMs mainly comes from (i) the hydrolysis of sulfonyl-containing linkages between perfluoroalkyl side chains and cationic end groups through nucleophilic substitution, or (ii) the degradation of cationic end groups *via* nucleophilic substitution or Hofmann elimination reactions. As mentioned earlier, both perfluoroalkyl side chains and cationic end groups are strongly electron-withdrawing, making sulfonyl-containing linkages between them especially vulnerable to nucleophilic attack by hydroxide ions. Overall, sulfonate esters are more prone to alkaline hydrolysis than sulfonamides because sulfonate esters are better leaving groups in nucleophilic substitution reactions.[57,58] This explains why Aquivion-SO_2NH-6CIm and Aquivion-SO_2NH-6CPip, which contain sulfonamide linkages, did not hydrolyze into Aquivion-SO_3H after alkaline treatment, unlike Aquivion-SO_3-2CIm and Aquivion-SO_2N-Im. In the case of Aquivion-SO_2N-Im, its sulfonyl linkage is directly attached to electron-deficient 1,2-dimethylimidazolium cations, making it especially vulnerable to hydroxide attack.[25,27] By contrast, the sulfonate ester linkage in Aquivion-SO_3-2CIm is likely stabilized by the adjacent ethyl spacer,[32] which may account for the slightly higher alkaline stability of Aquivion-SO_3-2CIm relative to Aquivion-SO_2N-Im.

In addition to the linkages, the cationic end groups in perfluorinated AEMs must also possess sufficient resistance to alkaline degradation to ensure the membrane performance in AEMWEs or AEMFCs. Park *et al.* previously reported that a hexyl spacer provides a higher energy barrier against Hofmann elimination degradation of quaternary ammonium end groups in perfluorinated AEMs compared to shorter alkyl spacers.[30] Accordingly, the hexyl spacers in Aquivion-SO_2NH-6CIm and Aquivion-SO_2NH-6CPip not only distance their cationic end-groups from the perfluoroalkyl side chain but also help stabilize these end-groups to some extent. More recently, N. Xie *et al.* reported that the lowest unoccupied molecular orbital (LUMO) energy of hexyl *N*-methylpiperidinium is higher than that of hexyl 1,2-dimethylimidazolium based on density functional theory (DFT) calculations, suggesting that hexyl *N*-methylpiperidinium is less susceptible to hydroxide attack.[59] These findings reasonably explain why the Aquivion-SO_2NH-6CPip AEM containing hexyl *N*-methylpiperidinium units exhibited better alkaline stability than the Aquivion-SO_2NH-6CIm AEM containing hexyl 1,2-dimethylimidazolium units.

3.4. Ionic conductivities of Aquivion-based perfluorinated anion exchange membranes

Ionic conductivity plays a critical role in determining the performance of AEMs in practical electrochemical applications. To avoid the influence of alkaline hydrolysis, the ionic conductivity of Aquivion-based perfluorinated AEMs was measured in the Cl^- form, which was prepared by immersing the membranes in a 1 M NaCl solution for 24 h prior to measurement. As shown in Fig. 5a, the chloride ion conductivities of these AEMs increased with temperature in the range of 30–80 °C and were strongly dependent on their IEC values. Among them, the Aquivion-SO_2N-Im AEM with the highest IEC (0.91 mmol g^{-1}) exhibited the highest chloride ion conductivity (9.4×10^{-3} S cm^{-1} at 80 °C), whereas the Aquivion-SO_2NH-

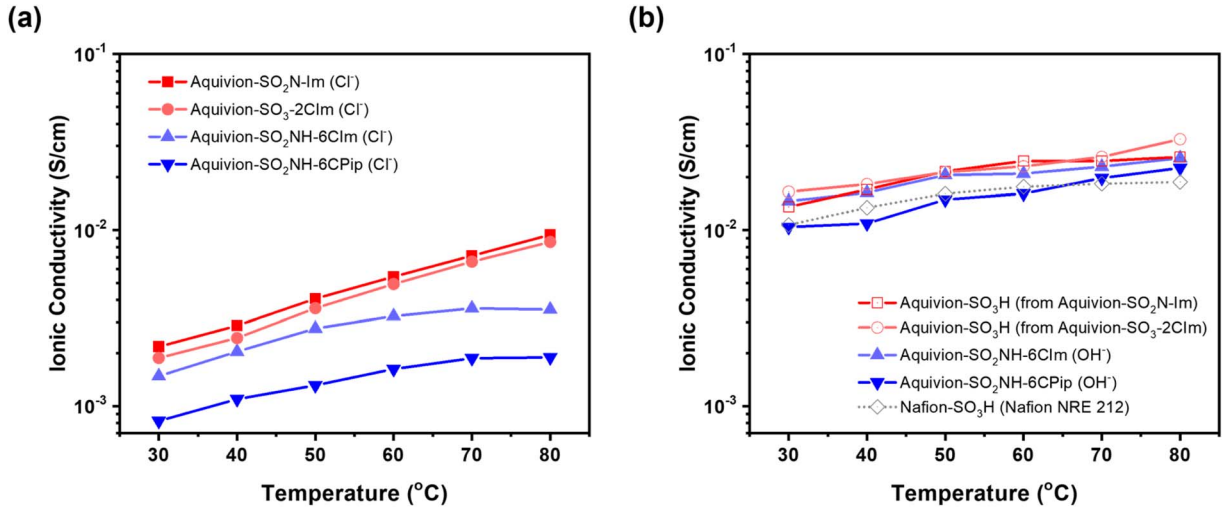

Fig. 5 Temperature-dependent ionic conductivities of perfluorinated polymer membranes (a) before and (b) after immersing in 1 M KOH at room temperature for 24 h.

6CPip AEM with the lowest IEC (0.31 mmol g^{-1}) showed the lowest conductivity (1.9×10^{-3} S cm^{-1} at 80 °C). On the other hand, the effective chloride-ion mobilities of our Aquivion-based perfluorinated AEMs were estimated at 30 °C using the method proposed by P. Knauth. The estimated values were 3.54×10^{-6} cm^2 V^{-1} s^{-1} for Aquivion-SO_2N-Im, 3.09×10^{-6} cm^2 V^{-1} s^{-1} for Aquivion-SO_3-2CIm, 2.40×10^{-6} cm^2 V^{-1} s^{-1} for Aquivion-SO_2NH-6CIm, and 9.67×10^{-7} cm^2 V^{-1} s^{-1} for Aquivion-SO_2NH-6CPip. These effective chloride-ion mobilities are comparable to those reported for PPO-based AEMs by P. Knauth *et al.* and are substantially lower than the chloride-ion mobility in infinitely diluted aqueous solution (7.9×10^{-4} cm^2 V^{-1} s^{-1} at 25 °C), which can be primarily attributed to the tortuosity of the hydrated ion-conducting channels within the membranes.[40]

Since the dimethylimidazolium end groups of Aquivion-SO_2N-Im and Aquivion-SO_3-2CIm underwent alkaline hydrolysis to form sulfonic acid groups, these two AEMs were converted into Aquivion-SO_3H PEMs after immersion in 1 M KOH for 24 h. In contrast, under the same alkaline conditions, Aquivion-SO_2NH-6CIm and Aquivion-SO_2NH-6CPip remained as AEMs and underwent ion exchange from Cl^- to OH^-. Following alkaline hydrolysis or ion exchange, the ionic conductivities of all membranes increased markedly to values exceeding 10^{-2} S cm^{-1} (Fig. 5b), comparable to that of the commercial PFSA PEM, Nafion NRE 212.

The Aquivion-SO_2NH-6CIm AEM exhibited a higher hydroxide ion conductivity (2.56×10^{-2} S cm^{-1} at 80 °C) and a lower activation energy for ion transport (9.8 kJ mol^{-1}) than Aquivion-SO_2NH-6CPip (2.25×10^{-2} S cm^{-1} at 80 °C and 14.5 kJ mol^{-1}, respectively), as presented in Table 2 and Fig. 6a. This can be attributed to the more well-defined hydrophilic/hydrophobic phase-separated nanostructure of Aquivion-SO_2NH-6CIm, as evidenced by the SAXS diffraction patterns (Fig. 6b), and TEM micrographs (Fig. 7). Aquivion-SO_2NH-6CIm ($\lambda = 8.7$) displayed two SAXS peaks corresponding to the *d*-spacing of nanodomains (~8.6 nm) and the nanodomain size (~2.8 nm), whereas Aquivion-SO_2NH-6CPip ($\lambda = 6.3$) showed no such peaks. Moreover, the hydrophilic nanodomains in the TEM micrograph of Aquivion-SO_2NH-6CPip appeared relatively ill-defined. These observations are consistent with the well-known cluster-network model, which predicts that PFSA membranes form continuous ion-conducting channels through the coalescence of ion clusters once the hydration number (λ) exceeds 7.[11,60]

In terms of elastic modulus, tensile strength, and strain at break (Table 2), Aquivion-SO_2NH-6CPip exhibited slightly better mechanical properties than Aquivion-SO_2NH-6CIm, primarily due to its relatively lower water uptake (WU). Both membranes, in the fully hydrated state, are sufficiently robust for practical applications, as their elastic moduli (0.33 and 0.75 GPa) and tensile

Table 2 Ionic conductivities and mechanical properties of the Aquivion-SO_2NH-6CIm and Aquivion-SO_2NH-6CPip AEMs

	Ionic conductivity at 80 °C (mS cm^{-1})					
Membrane code	Cl^- form[a]	OH^- form[b]	E_a[c] (kJ mol^{-1})	Elastic modulus[d] (GPa)	Tensile strength[d] (MPa)	Strain at break[d] (%)
Aquivion-SO_2NH-6CIm	3.5	25.6	9.8	0.33 ± 0.08	31.2 ± 1.6	21.6 ± 5.1
Aquivion-SO_2NH-6CPip	1.9	22.5	14.5	0.75 ± 0.16	48.2 ± 2.5	12.4 ± 3.5

[a] Before measurement, the AEM was immersed in 1 M NaCl at RT for 24 h to ensure itself in Cl^- form. [b] Before measurement, the AEM was immersed in 1 M KOH at RT for 24 h to ensure itself in OH^- form. [c] The activation energy was calculated from the slope of the Arrhenius plot of hydroxide ion conductivity. [d] All the membrane samples for the tensile test were fully hydrated.

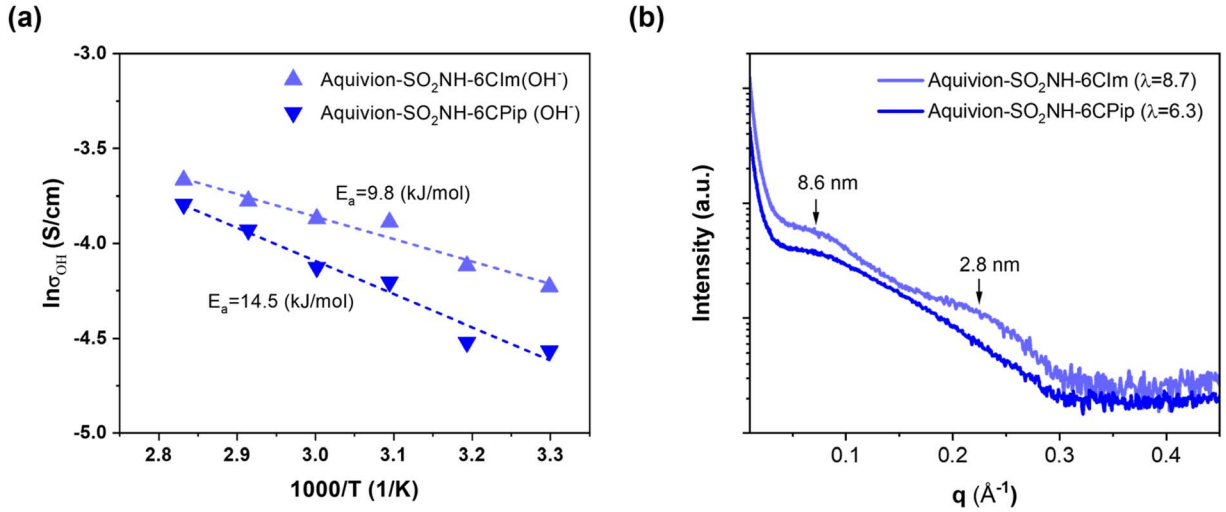

Fig. 6 (a) Arrhenius plots of hydroxide ion conductivity, and (b) SAXS diffraction patterns of the Aquivion-SO_2NH-6CIm and Aquivion-SO_2NH-6CPip AEMs.

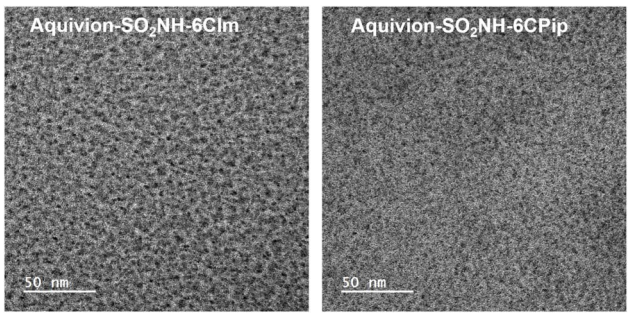

Fig. 7 TEM micrographs of the Aquivion-SO_2NH-6CIm and Aquivion-SO_2NH-6CPip AEMs.

strengths (31.2 and 48.2 MPa) are significantly higher than those reported previously for the commercial Nafion NRE 212 membrane (0.086 GPa elastic modulus and 12.7 MPa tensile strength).[61]

It is noteworthy that, after 192 h of alkaline treatment in 1 M KOH at 60 °C, the hydroxide ion conductivity of Aquivion-SO_2NH-6CPip (1.35×10^{-2} S cm^{-1}) was close to that of Aquivion-SO_2NH-6CIm (1.43×10^{-2} S cm^{-1}), as shown in Fig. 8. That is because the decline in hydroxide ion conductivity for Aquivion-SO_2NH-6CIm was more pronounced than for Aquivion-SO_2NH-6CPip. Specifically, Aquivion-SO_2NH-6CPip retained 83.8% of its initial ionic conductivity, whereas Aquivion-SO_2NH-6CIm retained only 68.5%. This result suggests that Aquivion-SO_2NH-6CPip exhibits better alkaline stability compared to Aquivion-SO_2NH-6CIm, in line with the TGA findings.

3.5. Water electrolysis performance

To further evaluate the applicability of Aquivion-SO_2NH-6CIm and Aquivion-SO_2NH-6CPip AEMs in electrochemical systems, we tested their performance in AEM water electrolysis (AEMWE)

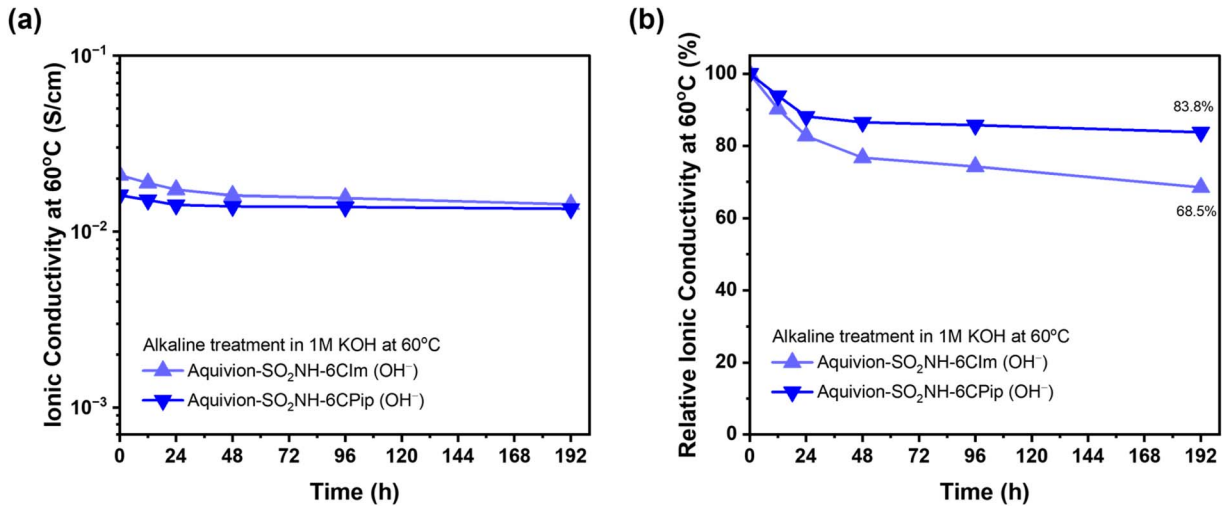

Fig. 8 Time-dependent (a) of hydroxide ion conductivity at 60 °C and (b) the corresponding ion conductivity retention relative to the initial value for the Aquivion-SO_2NH-6CIm and Aquivion-SO_2NH-6CPip AEMs during 192 h of alkaline treatment in 1 M KOH at 60 °C.

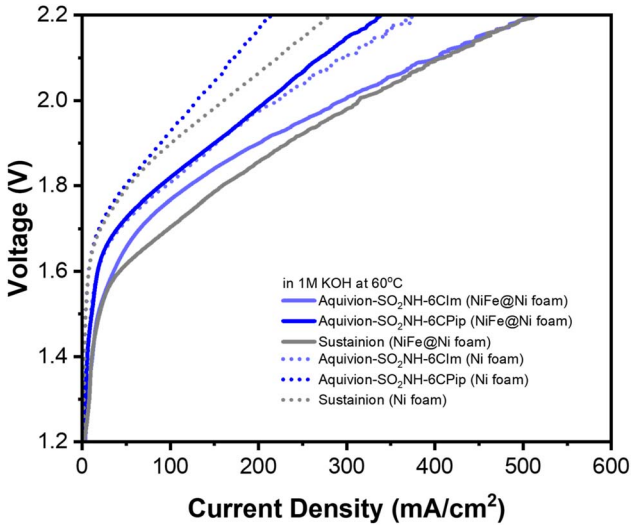

Fig. 9 Polarization curves of AEMWE for Aquivion-SO_2NH-6CIm, Aquivion-SO_2NH-6CPip, and Sustainion X37-RT AEMs in 1 M KOH at 60 °C using Ni foam electrodes (dot lines) and NiFe catalyst-coated Ni foam electrodes (solid lines).

using a zero-gap cell without noble metal catalysts. The polarization curves of AEMWEs based on these two Aquivion-derived AEMs and a commercial benchmark membrane, Sustainion X37-RT (Dioxide Materials, USA), recorded at 60 °C in 1 M KOH, are compared in Fig. 9. Aquivion-SO_2NH-6CIm exhibited superior AEMWE performance compared to Aquivion-SO_2NH-6CPip, likely due to its higher hydroxide ion conductivity. Using Ni foam electrodes, at 2.2 V, the current densities of Aquivion-SO_2NH-6CIm, Sustainion X37-RT, and Aquivion-SO_2NH-6CPip reached 317, 283, and 216 mA cm^{-2}, respectively. Notably, the performance of Aquivion-SO_2NH-6CIm was comparable to that of Sustainion X37-RT, indicating its strong potential for AEMWE.

Furthermore, coating the Ni foam electrodes with a NiFe catalyst *via* reductive deposition during a solvothermal reaction

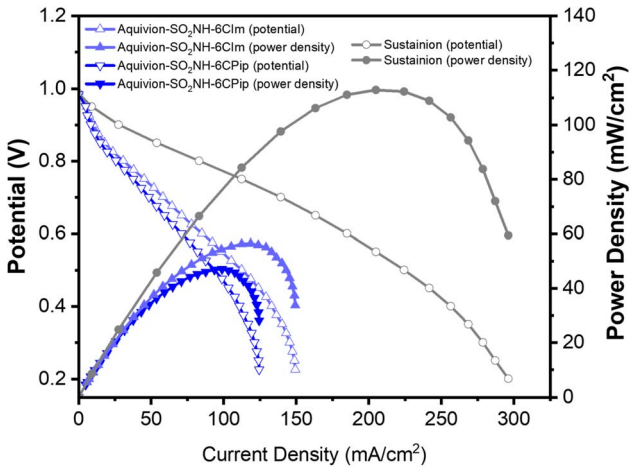

Fig. 10 Polarization curves of AEMFC operated at 60 °C under humidified hydrogen and oxygen for MEAs based on Aquivion-SO_2NH-6CIm, Aquivion-SO_2NH-6CPip, and Sustainion X37-RT AEMs.

remarkably enhanced the AEMWE performance of all membranes. The current densities at 2.2 V increased to 518, 512, and 339 mA cm^{-2} for Aquivion-SO_2NH-6CIm, Sustainion X37-RT, and Aquivion-SO_2NH-6CPip, respectively. Despite its relatively low IEC (0.34 mmol g^{-1}), Aquivion-SO_2NH-6CIm still delivered AEMWE performance comparable to that of a quaternary ammonium-functionalized Aquivion-based AEM (AQ720A-4, IEC = 0.92 mmol g^{-1}) reported recently by Carbone *et al.* (~555 mA cm^{-2} at 2.2 V and 60 °C).[62] These results demonstrate that sulfonamide-linked perfluorinated polymers with a hexyl spacer and 1,2-dimethylimidazolium or *N*-methylpiperidinium end groups are promising candidates as AEMs for practical applications, even at low degrees of functionalization.

3.6. Fuel cell performance

Fig. 10 compares the AEMFC performances of MEAs based on Aquivion-SO_2NH-6CIm, Aquivion-SO_2NH-6CPip, and Sustainion X37-RT AEMs. All fuel cells exhibited open-circuit voltages (OCVs) close to 1.0 V, indicating negligible gas crossover. Owing to its higher hydroxide conductivity, the MEA with Aquivion-SO_2NH-6CIm achieved a higher maximum power density (57 mW cm^{-2}) than that with Aquivion-SO_2NH-6CPip (47 mW cm^{-2}), as expected. However, both values were lower than that of the Sustainion X37-RT-based MEA (113 mW cm^{-2}). This difference can primarily be attributed to the much higher hydroxide conductivity of Sustainion X37-RT (6.67×10^{-2} S cm^{-1} at 60 °C)[63] compared with our Aquivion-based membranes. Additionally, the lower fuel cell performance of the Aquivion-based MEAs may also result from the commercial ionomer (Sustainion XB-7) used as the catalyst binder, which is likely more compatible with the Sustainion X37-RT membrane than with these Aquivion-based perfluorinated AEMs. Reduced interfacial compatibility at the catalyst–membrane interface can lead to less efficient electrochemical reactions at the fuel cell's triple-phase boundary.

4. Conclusions

We synthesized four Aquivion-based perfluorinated AEMs with different tethering structures (Aquivion-SO_2N-Im, Aquivion-SO_3-2CIm, Aquivion-SO_2NH-6CIm, and Aquivion-SO_2NH-6CPip) by varying combinations of sulfonyl-containing linkages, alkyl spacers, and nitrogen-based cyclic cationic groups *via* the SuFEx, Menshutkin, and S_N2 reactions. Due to their highly hydrophobic backbones and relatively low IEC values, all Aquivion-based perfluorinated AEMs exhibited excellent dimensional stability, with swelling ratios of less than 8.1%. Comparative analyses of FTIR and TGA indicated that the alkaline stability of these perfluorinated AEMs follows the order: Aquivion-SO_2N-Im < Aquivion-SO_3-2CIm < Aquivion-SO_2NH-6CIm < Aquivion-SO_2NH-6CPip. Both the sulfonyl and sulfonate ester linkages underwent hydrolytic cleavage under mild alkaline conditions (1 M KOH at room temperature), leading to the conversion of Aquivion-SO_2N-Im and Aquivion-SO_3-2CIm AEMs into perfluorinated PEMs. The ethyl spacer appeared to stabilize the sulfonate ester linkage in Aquivion-SO_3-2CIm to some extent, resulting in the slightly higher alkaline stability relative to Aquivion-SO2N-Im. In

contrast, the incorporation of a sulfonamide linkage combined with a longer hexyl spacer effectively suppressed alkaline hydrolysis in Aquivion-SO_2NH-6CIm and Aquivion-SO_2NH-6CPip. Owing to the higher intrinsic alkaline stability of the *N*-methylpiperidinium cation compared to the 1,2-dimethylimidazolium group, Aquivion-SO_2NH-6CPip exhibited higher hydroxide conductivity retention (83.8%) than Aquivion-SO_2NH-6CIm (68.5%) after 192 h of alkaline treatment in 1 M KOH at 60 °C. Nevertheless, Aquivion-SO_2NH-6CIm displayed slightly higher hydroxide conductivity (2.56×10^{-2} S cm^{-1} at 80 °C) than Aquivion-SO_2NH-6CPip (2.25×10^{-2} S cm^{-1} at 80 °C), due to its more well-defined hydrophilic/hydrophobic phase-separated nanostructure. Both Aquivion-SO_2NH-6CIm and Aquivion-SO_2NH-6CPip AEMs have demonstrated good potential for AEMWE and AEMFC applications. Notably, the Aquivion-SO_2NH-6CIm AEM exhibited great water electrolysis performance, reaching a high current density of 518 mA cm^{-2} at 2.2 V, which is comparable to that of the commercial Sustainion X37-RT membrane.

The major limitation of this study is the incomplete amination of the Aquivion-SO_2F precursor, which restricts the achievable degree of functionalization in the Aquivion-SO_2NH-6CIm and Aquivion-SO_2NH-6CPip AEMs. This limitation results in relatively low IECs and, consequently, lower hydroxide conductivities than those of highly functionalized AEMs. Future efforts should focus on developing alternative synthetic strategies to create sulfonamide-linked perfluorinated AEMs with alkyl spacers and alkaline-stable cationic end groups, without relying on the Aquivion-SO_2NH_2 precursor, to further improve membrane performance.

Conflicts of interest

There are no conflicts of interest to declare.

Data availability

The authors confirm that all relevant data supporting the findings of this study are included within the submitted manuscript. If any additional raw data files in alternative formats are needed, they can be made available upon reasonable request from the corresponding author.

Supplementary information (SI): preparation procedures for NiFe catalyst-coated Ni foam electrodes used in water electrolysis tests and gas diffusion electrodes for fuel cell tests; an additional ^{1}H–^{1}H COSY spectrum for material characterization; a schematic illustration of the possible zwitterionic behavior in Aquivion-based perfluorinated AEMs; and XPS and contact angle results of the Aquivion-based perfluorinated AEMs. See DOI: https://doi.org/10.1039/d5ra09534d.

Acknowledgements

The authors gratefully acknowledge the financial support of the National Science and Technology Council (Taiwan, R.O.C.) under project number MOST 111-2221-E-992-006-MY3. Besides, we acknowledge that the use of the Bruker Avance 600NMR spectrometer, ULVAC-PHI PHI 5000 VersaProbe XPS instrument, and Bruker Dimension ICON SPM instrument used herein belongs to the Instrument Center of National Cheng Kung University (NCKU). The authors also express their sincere thanks to Mrs Bi-Yun Lin at NCKU for her excellent assistance with the NMR analyses, Miss Chao-Jung Huang at NCKU for operating the XPS analysis, as well as to Mrs Shu-Jen Chen at Industrial Technology Research Institute (ITRI) for her outstanding support in performing the TEM observations.

References

1 A. Chrouda, A. Almoteiry, N. K. Al-Saleem, K. Slimi and H. F. Öztop, *Fuel*, 2026, **406**, 136858.
2 M. M. Hossain Bhuiyan and Z. Siddique, *Int. J. Hydrogen Energy*, 2025, **102**, 1026–1044.
3 J. G. Segovia-Hernández, S. Hernández, E. Cossío-Vargas, M. Juarez-García and E. Sánchez-Ramírez, *RSC Sustain.*, 2025, **3**, 134–157.
4 A. Javed, N. L. Wolf, F. Meyer, L. Treutlein, H. Kungl, A. Karl, E. Jodat and R.-A. Eichel, *Int. J. Hydrogen Energy*, 2025, **98**, 280–294.
5 S. J. Peighambardoust, S. Rowshanzamir and M. Amjadi, *Int. J. Hydrogen Energy*, 2010, **35**, 9349–9384.
6 D. W. Shin, M. D. Guiver and Y. M. Lee, *Chem. Rev.*, 2017, **117**, 4759–4805.
7 S. H. Kwon, H. Kang, J. H. Lee, S. Shim, J. Lee, D. S. Lee, C. M. Kim and S. G. Lee, *Mater. Today Commun.*, 2019, **21**, 100625.
8 S.-H. Shin, P. J. Nur, A. Kodir, D.-H. Kwak, H. Lee, D. Shin and B. Bae, *ACS Omega*, 2019, **4**, 19153–19163.
9 L. Ma, X. Liu, R. Yang, B. Guo, L. Zhou and Z. Zhao, *Fuel*, 2026, **405**, 136789.
10 K. A. Mauritz and R. B. Moore, *Chem. Rev.*, 2004, **104**, 4535–4586.
11 A. Kusoglu and A. Z. Weber, *Chem. Rev.*, 2017, **117**, 987–1104.
12 N. Li and M. D. Guiver, *Macromolecules*, 2014, **47**, 2175–2198.
13 R. Abbasi, B. P. Setzler, S. Lin, J. Wang, Y. Zhao, H. Xu, B. Pivovar, B. Tian, X. Chen, G. Wu and Y. Yan, *Adv. Mater.*, 2019, **31**, 1805876.
14 I. Vincent and D. Bessarabov, *Renew. Sustain. Energy Rev.*, 2018, **81**, 1690–1704.
15 J. Hyun and H.-T. Kim, *Energy Environ. Sci.*, 2023, **16**, 5633–5662.
16 D. Agrawal, N. Mahajan, S. A. Singh and I. Sreedhar, *Fuel*, 2024, **359**, 130131.
17 J. R. Varcoe, P. Atanassov, D. R. Dekel, A. M. Herring, M. A. Hickner, P. A. Kohl, A. R. Kucernak, W. E. Mustain, K. Nijmeijer, K. Scott, T. Xu and L. Zhuang, *Energy Environ. Sci.*, 2014, **7**, 3135–3191.
18 E. J. Park, P. Jannasch, K. Miyatake, C. Bae, K. Noonan, C. Fujimoto, S. Holdcroft, J. R. Varcoe, D. Henkensmeier, M. D. Guiver and Y. S. Kim, *Chem. Soc. Rev.*, 2024, **53**, 5704–5780.
19 F. Xu, Y. Su and B. Lin, *Front. Mater.*, 2020, **7**, 4.
20 X. Kong, K. Wadhwa, J. G. Verkade and K. Schmidt-Rohr, *Macromolecules*, 2009, **42**, 1659–1664.

21 M.-s. J. Jung, C. G. Arges and V. Ramani, *J. Mater. Chem.*, 2011, **21**, 6158–6160.
22 H. L. S. Salerno, F. L. Beyer and Y. A. Elabd, *J. Polym. Sci., Part B: Polym. Phys.*, 2012, **50**, 552–562.
23 H. L. S. Salerno and Y. A. Elabd, *J. Appl. Polym. Sci.*, 2013, **127**, 298–307.
24 X. Luo, D. I. Kushner and A. Kusoglu, *J. Membr. Sci.*, 2023, **685**, 121945.
25 K. Matsui, E. Tobita, K. Sugimoto, K. Kondo, T. Seita and A. Akimoto, *J. Appl. Polym. Sci.*, 1986, **32**, 4137–4143.
26 D. S. Kim, C. H. Fujimoto, M. R. Hibbs, A. Labouriau, Y.-K. Choe and Y. S. Kim, *Macromolecules*, 2013, **46**, 7826–7833.
27 C. G. Arges, M.-S. Jung, G. Johnson, J. Parrondo and V. Ramani, *ECS Trans.*, 2019, **41**, 1795–1816.
28 A. Bosnjakovic, M. Danilczuk, S. Schlick, P. N. Xiong, G. M. Haugen and S. J. Hamrock, *J. Membr. Sci.*, 2014, **467**, 136–141.
29 S. Lee, H. Lee, T.-H. Yang, B. Bae, N. A. T. Tran, Y. Cho, N. Jung and D. Shin, *Membranes*, 2020, **10**, 306.
30 A. M. Park, Z. R. Owczarczyk, L. E. Garner, A. C. Yang-Neyerlin, H. Long, C. M. Antunes, M. R. Sturgeon, M. J. Lindell, S. J. Hamrock, M. Yandrasits and B. S. Pivovar, *ECS Trans.*, 2017, **80**, 957–966.
31 X. Liu, H. Gao, X. Chen, Y. Hu, H. Li and Y. Zhang, *Polym. Chem.*, 2016, **7**, 2904–2912.
32 X. Liu, H. Gao, X. Chen, Y. Hu, S. Pei, H. Li and Y. Zhang, *J. Membr. Sci.*, 2016, **515**, 268–276.
33 X. Liu, D. Wu, X. Liu, X. Luo, Y. Liu, Q. Zhao, J. Li and D. Dong, *Electrochim. Acta*, 2020, **336**, 135757.
34 C. G. Arges and L. Zhang, *ACS Appl. Energy Mater.*, 2018, **1**, 2991–3012.
35 X. Lin, J. R. Varcoe, S. D. Poynton, X. Liang, A. L. Ong, J. Ran, Y. Li and T. Xu, *J. Mater. Chem. A*, 2013, **1**, 7262.
36 K. M. Hugar, W. You and G. W. Coates, *ACS Energy Lett.*, 2019, **4**, 1681–1686.
37 B. Lin, F. Xu, Y. Su, J. Han, Z. Zhu, F. Chu, Y. Ren, L. Zhu and J. Ding, *ACS Appl. Energy Mater.*, 2020, **3**, 1089–1098.
38 H.-S. Dang and P. Jannasch, *J. Mater. Chem. A*, 2017, **5**, 21965–21978.
39 L.-C. Jheng, W.-Y. Chen, G.-L. Huang, Z.-L. Zhao, S. L.-C. Hsu and W.-C. Ko, *Int. J. Hydrogen Energy*, 2025, **130**, 108–118.
40 P. Knauth, L. Pasquini, R. Narducci, E. Sgreccia, R. A. Becerra-Arciniegas and M. L. Di Vona, *J. Membr. Sci.*, 2021, **617**, 118622.
41 Z. Geng, J. J. Shin, Y. Xi and C. J. Hawker, *J. Polym. Sci.*, 2021, **59**, 963–1042.
42 V. Bisla and H. Yoshitake, *Carbohydr. Polym. Technol. Appl.*, 2024, **7**, 100462.
43 S. Bonizzoni, P. Stilli, F. Lohmann-Richters, C. Oldani, C. Ferrara, A. Papagni, L. Beverina and P. Mustarelli, *Chemelectrochem*, 2021, **8**, 2231–2237.
44 J. Wang, Z. Yang, J. Wang, C. Fan, D. Peng, L. Jin, F. Chen, Y. Xiang, Y. Su, X. Yang, Y. Pang, H. Chen, X. Zheng, Z. Shen and S. Wu, *Chem. Eng. J.*, 2025, **511**, 161995.
45 L.-C. Jheng, C.-W. Cheng, K.-S. Ho, S. L. Hsu, C.-Y. Hsu, B.-Y. Lin and T.-H. Ho, *Polymers*, 2021, **13**(17), 2864.
46 Y. Jiang, C. Shen, J. Chen, H. Lu, Y. Guo and S. Gao, *J. Appl. Polym. Sci.*, 2023, **140**, e54246.
47 M.-C. Ferrari, J. Catalano, M. Giacinti Baschetti, M. G. De Angelis and G. C. Sarti, *Macromolecules*, 2012, **45**, 1901–1912.
48 S. Lee, H. Lee, T.-H. Yang, B. Bae, N. A. Tran, Y. Cho, N. Jung and D. Shin, *Membranes*, 2020, **10**(11), 306.
49 Interpreting Infrared, Raman, in *Nuclear Magnetic Resonance Spectra*, ed. R. A. Nyquist, Academic Press, San Diego, 2001, pp. 85–117, DOI: 10.1016/B978-012523475-7/50185-6.
50 Z. Tao, C. Wang, X. Zhao, J. Li and Q. Ren, *Mater. Chem. Front.*, 2021, **5**, 6904–6912.
51 Y. Cho and H. Kang, *J. Environ. Chem. Eng.*, 2023, **11**, 109734.
52 A. G. Divekar, M.-C. Kuo, A. M. Park, A. R. Motz, Z. S. Page-Belknap, Z. Owczarczyk, H. Long, S. Seifert, C. M. Maupin, M. A. Yandrasits, Y. Yang, B. S. Pivovar and A. M. Herring, *J. Polym. Sci., Part B: Polym. Phys.*, 2019, **57**, 700–712.
53 G. H. A. Wijaya, K. S. Im and S. Y. Nam, *Desalination Water Treat.*, 2024, **320**, 100605.
54 S. Goswami, S. Klaus and J. Benziger, *Langmuir*, 2008, **24**, 8627–8633.
55 D. M. Hillman, S. H. Stephens, S. D. Poynton, S. Murphy, A. L. Ong and J. R. Varcoe, *J. Mater. Chem. A*, 2013, **1**, 1018–1021.
56 S. H. de Almeida and Y. Kawano, *J. Therm. Anal. Calorim.*, 1999, **58**, 569–577.
57 F. Duarte, T. Geng, G. Marloie, A. O. Al Hussain, N. H. Williams and S. C. Kamerlin, *J. Org. Chem.*, 2014, **79**, 2816–2828.
58 A. Białk-Bielińska, S. Stolte, M. Matzke, A. Fabiańska, J. Maszkowska, M. Kołodziejska, B. Liberek, P. Stepnowski and J. Kumirska, *J. Hazard. Mater.*, 2012, **221–222**, 264–274.
59 N. Xie, T. Wang, S. Du, Q. Weng, K. Zheng, T. Zhang, X. Ning, P. Chen, X. Chen and Z. An, *J. Power Sources*, 2023, **574**, 233121.
60 W. Y. Hsu and T. D. Gierke, *J. Membr. Sci.*, 1983, **13**, 307–326.
61 S. H. Kang, H. Y. Jeong, S. J. Yoon, S. So, J. Choi, T.-H. Kim and D. M. Yu, *Polymers*, 2023, **15**, 2109.
62 A. Carbone, S. C. Zignani, I. Gatto, R. Pedicini, C. Oldani, A. Cattaneo and A. S. Aricò, *Chem. Eng. J.*, 2023, **455**, 140765.
63 J. Eon Chae, J. Choi, S. Lee, C. Park and S. Kim, *J. Ind. Eng. Chem.*, 2024, **133**, 255–262.